Dynamics of End-Associated Triblock Copolymer Networks

Mai Nguyen-Misra and Wayne L. Mattice*

Institute of Polymer Science, The University of Akron, Akron, Ohio 44325-3909

Received May 16, 1995; Revised Manuscript Received July 12, 1995[⊗]

ABSTRACT: In this Monte Carlo study, the relaxation dynamics of transient networks formed by triblock copolymers via end association is followed. The stress relaxation moduli, deduced from the distributions of bridge lifetimes, are examined with focus on the effects of the system variables, including the solvent quality, concentration, the middle block size, and the end block size. In general, the stress in such systems decays, upon an application of a unit shear strain, as bridges, which supported the stress, convert to dangling ends (via the end-breaking mechanism) and loops (via the fusion mechanism). The transition rates of bridges to other states depend strongly on the interaction energy between the end block segments and the solvent molecules ($\beta\epsilon$) and the end block size but weakly on the middle block size and concentration. The bridge lifetime distribution does not fit a simple exponential function, leading to a stress decay that is also nonexponential. As $\beta\epsilon$ increases, the lifetime distribution becomes increasingly more nonexponential and its tail extends to longer lifetimes. The contributions from the slower modes become more significant as $\beta\epsilon$ increases, leading to larger average bridging lifetimes. On the other hand, as the end block size gets longer, the bridges, on average, have shorter lifetimes. The stress relaxation appears to fit a stretched-exponential decay. As $\beta\epsilon$ increases, the rubbery plateau region broadens and its height increases. The transition to flow occurs more slowly (as indicated by the larger slopes in the terminal zone) with increasing $\beta\epsilon$. As the end block size increases, both the width and height of the plateau region decrease. The transition to flow occurs at a faster rate, with longer end block size.

I. Introduction

The molecular origin for the interesting rheological behavior of transient networks is not yet well understood, mainly as the result of the complexity in the association or network formation process itself. Most of the recent theoretical models, developed under various simplifications, attempt to mimic real transient network systems, namely ionomers or polymers with randomly distributed hydrogen-bonding groups. On the experimental side, most of the existing studies on reversible networks have focused on the mechanical properties of various systems of urethane-linked ethylene oxide polymers with short hydrophobic end groups (associative thickeners),[1-4] polymers with hydrogen-bonding substituents,[5-8] and ionomers.[9,10]

The first set of theories on the dynamic aspects of transient networks was developed to explain the stress decay in viscoelastic polymeric systems.[11-13] These studies however were limited by the lack of detailed knowledge on the molecular mechanisms for the formation/annihilation of temporary junctions. In the model of Green and Tobolsky (GT), the original kinetic theory of elasticity (developed for conventional chemical networks) was extended to account for the continual breaking and re-forming of junctions in transient networks.[11] The most important feature in the GT model was its assumption of a single internal relaxation time, i.e., constant active chain breakage rate. The GT model was later modified independently by Lodge,[12] who allowed for multiple relaxation processes in the system, and by Yamamoto,[13] who considered the dependence of the active chain breakage probability on the chain conformation. Both models were developed to look at the dynamics of entangled melts, where the localized entanglements acted as temporary junctions. However, these models excluded the regeneration of active chains (from dangling ends) and thus could not predict the shear thickening and shear thinning phenomena observed at intermediate and high shear rates, respectively.

The more recent set of theories may be broadly classified into two groups: unentangled and entangled types. For an unentangled network, where the chain length, N, between two junctions is less than the entanglement chain length N_e ($N < N_e$), the network chain relaxation may be described by the modified Rouse model and the dynamics is essentially dependent on the breaking of the junctions. In an entangled network ($N > N_e$), the dynamics is considerably hindered by the presence of entanglements. The summary of these theories is also organized along those lines.

Tanaka and Edwards[14-17] (TE) and Wang,[18] respectively, addressed the time evolution of stress after a step strain had been applied to the network, in the unentanglement regime. TE modified the Yamamoto model to study transient networks formed by association of telechelic polymer chains with sticky ends. The system considered in the TE model was a melt of monodisperse polymer chains, with each chain having one interacting, or sticky, group at each end. Essentially, two types of chains were considered in this model: bridges (elastically active) and dangling ends (elastically inactive). The stress transfer by a dangling chain was made only through a viscous interaction, whose contribution was insignificant in comparison with the elastic contribution by the bridging chains and was not considered. The internal reorganization of the network and thus the network properties were determined essentially by two molecular parameters: the rates of breaking, $\beta(r)$, and recombination, p_B, of active chains. Due to the continual formation and annihilation of the bridging chains, the number of active chains varied with time. To account for the non-Newtonian behavior in steady shear, the breaking rate, $\beta(r)$, was allowed to vary with the end-to-end distance, r, of the bridges. This variable breaking rate leads to a variable viscosity, since chains stretched under shear. The nature of the flow curve under shear was sensitive to the choice of $\beta(r)$. The model was reduced to the GT[11] model in the limit where the chain breakage rate became independent of r. In addition, a

[⊗] Abstract published in *Advance ACS Abstracts,* September 1, 1995.

0024-9297/95/2228-6976$09.00/0

dangling chain had a probability, p_B, per unit time of capturing one of the neighboring junctions to become active. By combination of these two terms, a recursion relation, which related the chain distribution function at some time t to that of a previous time step, was generated. This recursion relation in continuous time resembled that derived by Yamamato for an entangled melt but differed in that the chain generation function in the TE model also depended on the number of active chains present at time t.

Wang's extension of the TE model allowed the dynamic exchange between bridging, dangling, and free chains.[18] This model showed that the shear-thickening phenomenon was governed by both the number of free chains present and the rate of formation of networked chains from free chains. To account for the shear-rate dependence of mechanical properties, the rates at which effective chains or free chains became dangling and vice verse were allowed to vary with shear rate. This model was reduced to the TE model in the limit where dangling chains could no longer become free.

Baxandall introduced a model to examine the motion of a polymer chain with sites that bind reversibly with a phantom network (i.e., absence of tubelike confinement effects), which itself had permanent cross-links.[19] The stress in the chains, after the network was strained, relaxed as the reversible cross-links between the chain and the host network broke and re-formed. In general, the length of the chain sections between cross-links was taken to be a variable with a spectrum of relaxation times associated with each section. This was a refinement over the simple theory of Lodge[12] which assumed only one relaxation mode for each chain section between cross-links. For chains with cross-links only at the two ends under a step strain, the time-evolution relaxation modulus was found to be exponential, i.e., exhibiting a single relaxation rate. As the number of cross-links increased, the relaxation of adjacent segments became correlated, resulting in slower relaxation.

Another set of theories, including the Gonzalez[20,21] and Leibler, Rubinstein, and Colby[22] (LRC) models, examined the relaxation of a chain with sites that bind reversibly with a host network, with entanglement effects incorporated. The diffusion of a networked chain was modeled using the tube (reptation) model of Doi and Edwards.[23] The qualitative disagreements in the two models arose from the different approaches the authors used to model the effects of those reversible ties on the mobility of the chain. The most crucial assumption in the Gonzalez model was that a chain could not reptate unless it was completely free of all cross-links; this led to an overestimation of the terminal relaxation times. LRC showed that a breaking of only a few cross-links was enough for a chain to relax considerably, a prediction that was in closer agreement with experimental observations.[5-8] The LRC model predicted a self-diffusion coefficient that was significantly higher than that given by the Gonzalez model, although still much smaller than that obtained from the modified Rouse model.

The relaxation dynamics of the transient networks formed via end association of the triblock copolymer chains is the focus of this Monte Carlo study. In an earlier study, we have observed that, under certain conditions, a 3-dimensional network may be formed by triblock copolymers in a medium that is a nonsolvent for the end blocks.[24] The micelle-like clusters, which act as temporary cross-links, are formed by association of the end blocks. The equilibrium behavior of such systems was studied in an earlier work. The dynamic properties of these systems are under investigation in this study. To understand the effects of the relevant system variables on the network relaxation, the lifetime distributions of the bridges were determined. The variable parameters under investigation include the number of segments per end block and middle block, the solvent selectivity, and the copolymer concentration.

This paper is organized into four sections. Following the Introduction, the simulation details are described in section II. This section presents the ranges of parameters investigated in the simulations as well as the details of how the dynamics of the chains was followed. The discussion of results, which follows in section III, is organized into two parts. First the lifetime distribution of bridges, along with the average bridging lifetime, is discussed in terms of their dependence on the variables. The equilibrium properties that are pertinent to the discussion of the dynamics, including the weight-average micellar aggregation number, p, number of micelles in the simulation box, n, equilibrium bridging fraction, f_b, micellar compactness, and average number of bridges per micelle, are also briefly reviewed in this section. Part 2 of this section presents the stress relaxation moduli, as deduced from the bridge lifetime distributions. Conclusions are presented in section IV.

II. Simulation Model

1. System Variables. The dynamics trajectory was generated in a manner similar to that in the equilibrium investigation of this system.[24] The simulations were performed on a cubic lattice of size $L = 40$, with periodic boundary conditions imposed in all three directions. This box size was chosen for the reasons that were discussed in detail elsewhere, namely with regard to simulation time and lattice size effects.[24]

To summarize, the voids were taken to be an athermal solvent (S) for the middle (B) block and a nonsolvent for the end (A) blocks. The only nonzero energy terms were those between the A segments with the B segments and the voids. Both were equal and repulsive, or $\beta\epsilon_{AS} = \beta\epsilon_{AB} = \beta\epsilon > 0$ and $\beta = 1/kT$. The parameters that were varied included concentration, ϕ, the end block size, N_A, the middle block size, N_B, and $\beta\epsilon$.

To study the concentration dependence, ϕ was varied from 0.03 to 0.14 with $N_A = 15$ and $N_B = 10$. $\beta\epsilon$ was kept constant at 0.1 or 1.0. This concentration range covered the system before and after it had gelled; the critical gel point under these conditions was estimated to be approximately 0.09 and 0.06, respectively, for $\beta\epsilon$ values of 0.1 and 1.0.

The effects of $\beta\epsilon$ on the dynamics were investigated at two concentrations, $\phi = 0.075$ and $\phi = 0.094$, using $N_A = 15$ and $N_B = 10$. The interaction energy was varied from 0.1 to 3.0 to cover both the weak and strong segregation regimes. Under these conditions, this system forms a 3-dimensional network.

The end block size dependence was characterized at two concentrations, below ($\phi = 0.038$) and above ($\phi = 0.094$) the gel point. The end block size was varied from 10 to 30 with $N_B = 10$. For the study at $\phi = 0.038$, $\beta\epsilon$ was varied such that the incompatibility parameter, $2N_A\beta\epsilon$, remained constant at 30. The investigation at $\phi = 0.094$ was carried out at two levels of incompatibility, in the weak and strong segregation ranges, or at $2N_A\beta\epsilon = 9$ and 30, respectively.

The middle block size effect was investigated with two different end block sizes, $N_A = 5$ and 15, at a concentration above the gel point ($\phi = 0.094$). Using an end block

size of 15, N_B was varied from 10 to 40 while $\beta\epsilon$ was fixed at 1.0. For the second set of study at an incompatibility of 10, a smaller end block size of 5 was used to obtain larger values of N_B, for 20 to 60. The total chain length was limited by simulation time and lattice size effects, as discussed elsewhere.[24]

2. Simulation Details. a. Equilibrium Ensemble. The equilibrium ensembles were generated as described in an earlier work. The types of moves used were the typical Monte Carlo moves including reptation, kink-jump, and crankshaft.[25,26] First, the chain to be moved was picked randomly and the chain end to be reptated was also chosen randomly. Reptation was allowed if the excluded volume condition and Metropolis rule were not violated (see refs 24 and 25 for more details). Subsequently, a segment on that chain was randomly chosen. If the chosen segment was an end segment, then again reptation was attempted. If it was an internal segment, then it was either kink-jumped or crankshafted, whichever was allowed. Ten million moves were attempted in order to generate the initial disordered state. The energy was then turned "on" and 5 million moves were made to generate the equilibrium structure. The averages were calculated for the last 50 configurations, with each pair separated by one Monte Carlo time steps (MCS), of a given trajectory; $M \times N$ attempted moves constituted one Monte Carlo time step, where M and N are the number of copolymer chains and the chain length, respectively. The equilibrium properties such as the average chain fraction (of bridge, loop, dangling, and free), micelle aggregation number, and micelle number density were used for cross-checking with those calculated using the dynamics trajectory. As part of the analysis of the dynamic properties, the average degree of micellar "looseness" was estimated as the fraction of nonbonded neighboring sites of associated (core) A blocks, that were occupied by the solvent molecules (or not occupied by either segment A or B).

b. Dynamics of Chains. The final configuration sampled in the equilibrium study was used as the initial configuration of the dynamics trajectory. In the dynamics run, three moves were allowed: end-flip, replacing the reptation move in the equilibrium study, kink-jump, and crankshaft.[25,26] Otherwise, the approach used in generating the dynamics trajectory was exactly the same as that used in generating the equilibrium ensembles. New configurations were generated by cycling between the end move, end-flip, and the internal moves, kink-jump or crankshaft as applicable. A chain to be end-flipped was chosen randomly. Following that, a randomly-chosen bead was either end-flipped if it was an end bead or kink-jumped or crankshafted if it was an internal bead. The self and mutual-avoidance conditions as well as the Metropolis rule were followed in accepting or rejecting a move.

Desired properties, including the state of each chain (bridge, loop, dangling, or free), the micelle aggregation number of each micelle, and the micelle number density, were calculated and stored for every MCS. The simulation box for each set of $\{\beta\epsilon, N_A, N_B, \phi\}$ was subjected to a dynamic run of 1500 Monte Carlo time steps (or 9×10^6 attempted moves for $\phi = 0.094$). At the end of each dynamic run, we thus had the history of each chain as a linear sequence of states from which the lifetime spectrum of any state could be extracted.

III. Results and Discussion

The dynamic behavior of the transient networks formed by association of triblock copolymers is examined in terms of its response to a small unit step strain. The weak nature of the van der Waals forces leads to a dynamic equilibrium between chains in the following four states: (i) free, (ii) dangling (one end block is a micelle while the other is dangling free in solution), (iii) loop (both end blocks are in the same micelle), and (iv) bridge (each end block is in a different micelle). Stress in this system relaxes by the conversion of the bridges to other states, through thermal fluctuations, fluctuations in the stretching of the bridging chains, and intermicellar interactions. The shear stress relaxation modulus for the system, in the linear regime, is predicted using the spectrum of lifetimes of bridges. In parts 1 and 2, we will look explicitly at the lifetime distribution of bridges and the manner in which it is affected by the solvent/end block interaction, polymer concentration, and the individual block size as well as its implication on the stress relaxation of these systems.

Figure 1. History of a chain as a linear sequence of states. At each Monte Carlo time step the chain is in one of the following states: bridge (B), loop (L), dangling end (D), or a free chain (F). Sequences of continuous bridging define a bridging event, and the number of time steps in the sequence defines a bridging time, τ.

1. Bridging Lifetime Distribution and Transition Rates. In section II, it was indicated that, in each dynamic run, the state of each chain was recorded at each time step. At any time, a chain is in any of the four states, including free, dangling, loop, or bridge. We thus have, at the end of a dynamic run, the history of each chain as a sequence of states, for each set $\{\beta\epsilon, N_A, N_B, \phi\}$. A specific illustration of the chain history is shown in Figure 1. The chain history can then be scanned for sequences of consecutive bridging states. Each such sequence corresponds to a bridging event, i.e. a chain forming a bridge and existing as a bridge for some time before converting to one of the other states. For each set of variables, one can obtain a set of bridging events, each with a different time span. From this set, the lifetime distribution of bridges, i.e. the probability distribution of finding a bridge with a particular lifetime, can be deduced. A similar analysis was done in the study of the dynamics of end-adsorbed copolymers.[27] Lifetime distributions of other states, including free, dangling, and loop, can be obtained in a similar manner. Additionally, the average bridging lifetime can then be estimated using the lifetime distribution of bridges.

A bridging chain could relax either by disassociating at one end (converting to a dangling end) or pulling the two interconnected micelles together (forming a loop). These mechanisms are illustrated in Figure 2. The corresponding rates of the two mechanisms depend on the environment surrounding the chain. The factors that need to be considered include the intermicellar interactions, the chain stretching, and the local friction and excluded volume forces felt by the associated end blocks. A bridging chain becomes a dangling chain when one of its two ends is expelled from a micelle with which it was associated, a relaxation process which is similar to that proposed for surfactant and diblock copolymer micelles.[28-31] This mechanism, referred to

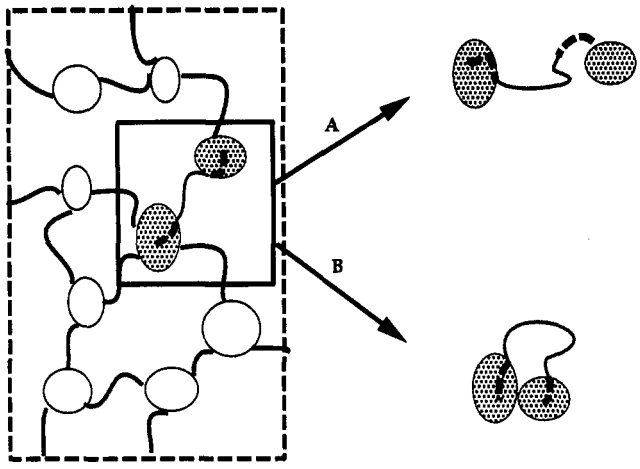

Figure 2. Mechanisms for relaxation of triblock copolymer bridges: (A) end breaking and (B) fusion.

as the end-breaking mechanism in our discussion later, is determined mainly by the compactness of the micellar cores with which these ends are associated, the average core dimension, the micellar aggregation number, and the stretching penalty. (In our simulations, a micelle is defined as a group of two or more chains having at least one A–A interchain contact; a bridging chain becomes a dangling chain when one of its A blocks no longer has any contacts with other A blocks). As the cores become more compact or larger in size (either in dimension or aggregation number, p), it will take a longer time for an A block to withdraw. A bridging chain will break, from one of its ends, as the tension in the chain exceeds the energy of association.

The second relaxation mechanism involves the conversion of bridges to loops by fusion or coalescence of the two micelles involved (Figure 2). This mechanism, which is peculiar mainly to systems that have bridging, is referred to as the fusion mechanism in our discussion. The bridging nature of the triblock copolymer chains which allows gel formation also leads to instability in the micelles (bridging attaction[32-37]). In our simulations, micellar fusion takes place when any one of the A segments belonging to one micellar core comes in contact with any of the A segments that are part of the other micellar core. The efficiency of this mechanism depends on a host of factors that define the attraction between micelles, including the number of bridges per micelle, $\langle n_b \rangle$, micellar aggregation number, p, and intermicellar distances. The attractive interaction results from an increase in entropy when copolymer chains are able to form bridges in addition to loops as the two micelles are close together. The attractive free energy is expected to be of the order of the number of bridges times kT. This attractive interaction competes with the repulsive interactions of the loops and dangling ends in the coronas of the two opposing micelles (similar to repulsive interactions by two opposing brushes). At short intermicellar distances, the repulsive part dominates. At larger distances, the attractive forces may dominate, inducing micellar coalescence.

There is also a small probability that a bridging chain could convert directly to a free state. However, the relaxation of bridges via this mechanism is insignificant, as compared to the breaking and the fusion mechanisms and is not considered in our analysis.

The number-averaged bridging lifetime, $\langle \tau_B \rangle$, in units of Monte Carlo time steps [MCS], and the rates of transition [$(MCS)^{-1}$ per chain] from bridges to loops (fusion) and bridges to dangling ends (breaking), respectively, are reported in this section. In the analysis of the bridging lifetime distribution, the bridging events were assigned to 30 bins of equal time interval, $\Delta\tau$, between $\tau = 0$ and $\tau = \tau_{max}$, where τ_{max} is the largest bridging time observed for that set of parameters and $\Delta\tau = \tau_{max}/30$. Equation 1 shows how $\langle \tau_B \rangle$ is calculated.

$$\langle \tau_B \rangle = \sum_i \tau_i P(\tau_i) \Delta\tau \qquad (1)$$

Here τ_i is the intermediate lifetime value in interval i, the normalized probability of finding a bridge with lifetime τ_i, $P(\tau_i)$, is $n_B(\tau_i)/(\Delta\tau \sum n_B(\tau_i))$, and $n_B(\tau_i)$ is the number of bridging events having lifetimes between $(\tau_i - \Delta\tau/2)$ and $(\tau_i + \Delta\tau/2)$.

The equilibrium properties, including p, n, and average number of bridges per micelle (equivalent to the average functionality of the system), are relevant to the interpretation of the dynamics and so are reviewed once again in this section. These equilibrium properties were determined using the current dynamic trajectories and were found to be in complete agreement with those calculated using the equilibrium ensembles. The fraction of nonbonded neighboring sites of the associated A blocks that were occupied by the solvent molecules is used in this study as a rough index of degree of "looseness" in the micellar cores; this index is referred to as the "looseness" factor, LF, throughout our discussion. A more accurate analysis of the micellar compactness would require a detailed calculation of the density profile in the micelles. Nevertheless, the looseness factor estimated here provides a rough estimate of how loose the micelles are, which has a direct consequence on the breaking rate of the bridges.

a. Effects of Energy of Interaction. In a previous study, we have shown that the micellar aggregation number is broadly distributed, particularly at high concentrations. At high concentrations, when micellar coalescence (due to the bridging attraction) has already taken place, the weight-average micelle aggregation number, p, is seen to be strongly dependent on $\beta\epsilon$. The micelles become more polydisperse in size as $\beta\epsilon$ increases and vice versa.

In panel a of Figure 3, the effects of $\beta\epsilon$ on the looseness factor of the micelles are illustrated, for $\phi = 0.075$ and 0.094, respectively. The micellar core becomes more compact as $\beta\epsilon$ increases, a qualitative trend that has also been observed in diblock copolymer micelles. As the environment becomes a poorer solvent for the core (A) blocks, the A cores become more compact in size to minimize their interactions with the solvent molecules.

The average number of bridges per micelle, $\langle n_b \rangle$, a factor which is important in gauging the average attraction between micelles, is shown as a function of $\beta\epsilon$, in panel b of Figure 3. The average number of bridges per micelle (or the average functionality of the system) is calculated as $\langle n_b \rangle = 2Mf_b/n$, where M, f_b, and n are the number of copolymer chains, the equilibrium bridging fraction, and the number of micelles in the system, respectively. The bridging fraction was seen to increase with incompatibility while the micelle number density exhibited a minimum at $2\beta\epsilon N_A \sim 5.0$ (or $\beta\epsilon \sim 0.2$). Both leveled off at high incompatibility. Panel b of Figure 3 shows that $\langle n_b \rangle$ initially increases almost linearly as $\beta\epsilon$ increases, reaching a plateau value at $\beta\epsilon \sim 0.7$ when $\phi = 0.094$.

In Figure 4, the effects of $\beta\epsilon$ on the fusion, breaking, and total rate, respectively, for ϕ of 0.094, are examined.

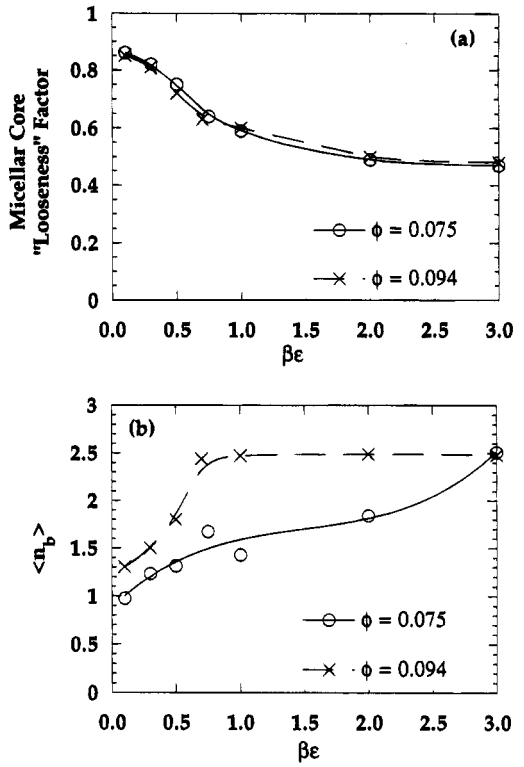

Figure 3. Effects of $\beta\epsilon$ on (a) the micellar core "looseness" factor and (b) $\langle n_b \rangle$ for $N_A = 15$, $N_B = 10$, and $\phi = 0.075$ (○) and 0.094 (×).

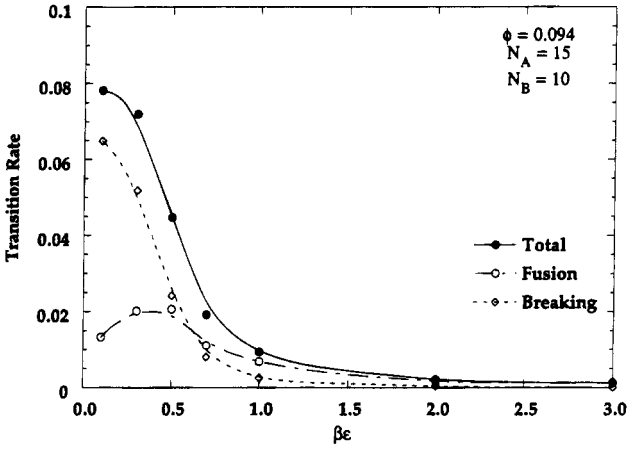

Figure 4. Variations in transition rate with $\beta\epsilon$ for $N_A = 15$, $N_B = 10$, and $\phi = 0.094$. The lines are drawn for visual guides.

Similar qualitative trends are also observed for $\phi = 0.075$. As expected, the breaking rate decays rapidly as $\beta\epsilon$ increases, dropping more than 10-fold to about 4 $\times 10^{-3}$ MCS^{-1} at $\beta\epsilon \sim 1$. As $\beta\epsilon$ increases, the micelles become more compact with increasing energy, and thus more time is required for the associated end block to withdraw from the micellar core. The fusion rate passes through a maximum, as $\beta\epsilon$ increases. At low to intermediate $\beta\epsilon$, the fusion rate increases as $\beta\epsilon$ increases, due to an increase in both p and $\langle n_b \rangle$. As $\beta\epsilon$ increases further, p decreases (while $\langle n_b \rangle$ remains constant), leading to a decrease in the fusion rate. In addition, this figure illustrates that bridges relax predominantly via the breaking mechanism, at low $\beta\epsilon$. At high $\beta\epsilon$, the relaxation of bridges occurs predominantly by the fusion mechanism. The crossover occurs at $\beta\epsilon \sim 0.7$. The combination of the two rates produces an overall decrease in the total rate, as $\beta\epsilon$ increases. Possibly due to the occurrence of the fusion mechanism, the overall rate decreases nonexponentially.

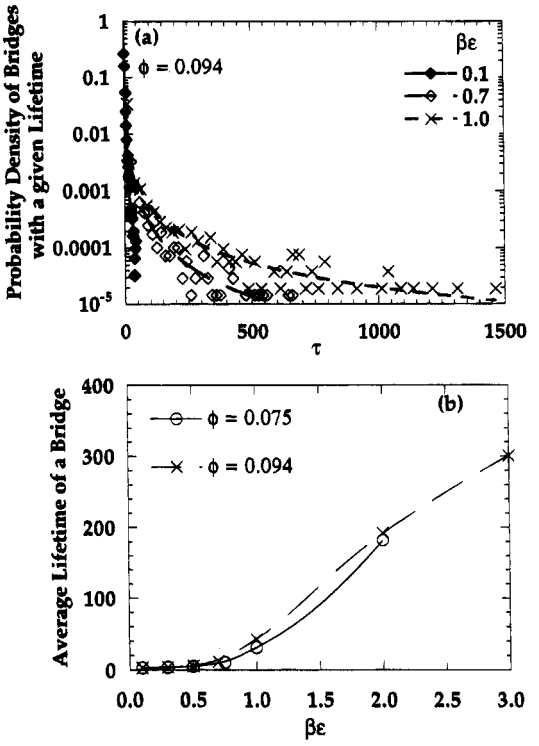

Figure 5. (a) Normalized probability density of a bridge with a given lifetime τ, for $\phi = 0.094$ and various values of $\beta\epsilon$. (b) $\langle \tau_B \rangle$ as a function of $\beta\epsilon$.

In panel a of Figure 5, the lifetime distributions of bridges are depicted, in a semilog plot, for various values of $\beta\epsilon$ and $\phi = 0.094$. The curves shown in this figure are from the best power-law fits to the data and presented only as visual guides. This figure illustrates, as expected, that the distribution does not follow a simple exponential decay. The distribution becomes increasingly more nonexponential, as $\beta\epsilon$ increases. At first glance, it may appear in panel a that the distributions at low energies are exponential, but further analysis shows that they are not. In addition, as $\beta\epsilon$ increases, the tail extends to longer lifetimes and the contributions of the slower relaxation modes also become more significant. The nonexponential decay in the lifetimes of bridges may be attributed to a number of factors, including the polydispersity in the micelle aggregation number and micellar structure and the existence of more than one relaxation pathway (i.e., breaking and fusion). In panel b of Figure 5, the average bridging lifetime, $\langle \tau_B \rangle$, is shown as a function of $\beta\epsilon$. At low $\beta\epsilon$, the total transition rate of bridges to other states is large, resulting in short bridging lifetimes. At high $\beta\epsilon$, the reverse is true. As $\beta\epsilon$ increases, $\langle \tau_B \rangle$ increases slowly at low $\beta\epsilon$, rising more rapidly at high $\beta\epsilon$.

b. Effects of Copolymer Concentration. Previously, it was also shown that p is insensitive to concentration, at low concentrations, but rises rapidly with concentration, once a certain concentration is reached.[24] Likewise, the micellar size polydispersity also varies with concentration in a similar manner. Panel a of Figure 6 shows almost no change in the micellar compactness as ϕ increases, over a wide range of ϕ. On the other hand, the micelle number density initially increases linearly with increasing ϕ, leveling off at higher ϕ, and the bridging fraction increases monotonically with concentration. In panel b of Figure 6, the effects of concentration on $\langle n_b \rangle$ are examined, at $\beta\epsilon = 0.1$ and 1.0. As expected, $\langle n_b \rangle$ increases with

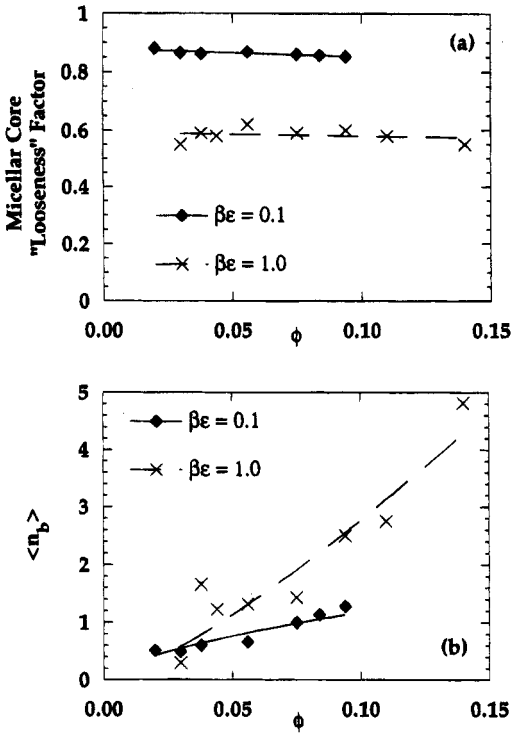

Figure 6. Effects of ϕ on (a) the micellar core "looseness" factor and (b) $\langle n_b \rangle$ for $N_A = 15$, $N_B = 10$, and $\beta\epsilon = 0.1$ (◆) and 1.0 (×).

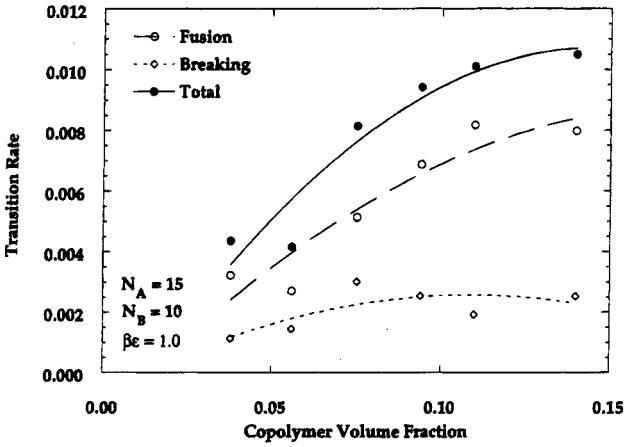

Figure 7. Variations in transition rate with ϕ for $N_A = 15$, $N_B = 10$, and $\beta\epsilon = 1.0$. The lines are drawn for visual guides.

concentration, increasing more rapidly at higher energies.

The transition rates are shown as a function of ϕ in Figure 7, for $\beta\epsilon = 1.0$. At $\beta\epsilon = 1.0$, the micelles are compact, making it difficult for the bridging end to withdraw, and more bridges convert to loops by fusion rather than to dangling ends by breakage. Correspondingly, Figure 7 shows that the fusion rate dominates over the whole range of ϕ investigated. As ϕ increases, the number of bridges per micelle increases, leading to an increase in the fusion rate. Since micellar compactness is insensitive to ϕ (Figure 6a), there is almost no change in the breaking rate as ϕ increases.

In panel a of Figure 8, the lifetime distributions of bridges are shown, for various concentrations at $\beta\epsilon = 1.0$. Panel b of the same figure illustrates the effects of concentration on the average bridging lifetime, for $\beta\epsilon = 0.1$ and 1.0. Panel a shows that there is extensive overlapping of data, for distributions at different concentrations, and the differences could not be resolved. Panel b shows that, for $\beta\epsilon = 1.0$, the average bridging

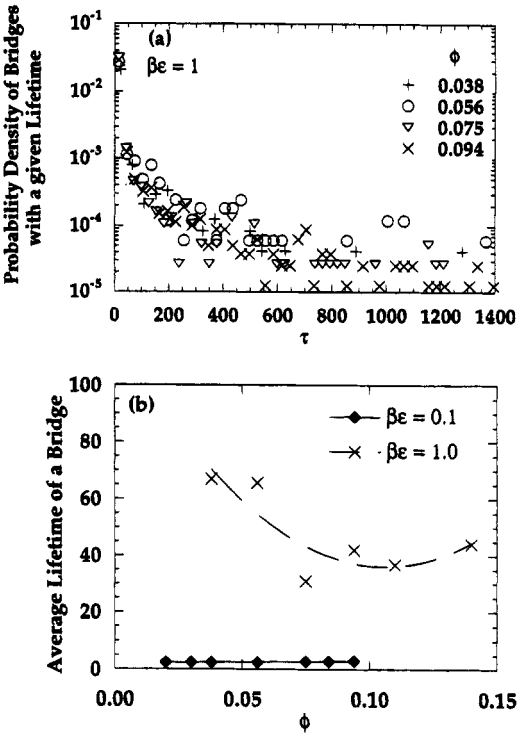

Figure 8. (a) Normalized probability density of a bridge with a given lifetime τ, for $\beta\epsilon = 1.0$ and various values of ϕ. (b) $\langle \tau_B \rangle$ as a function of ϕ.

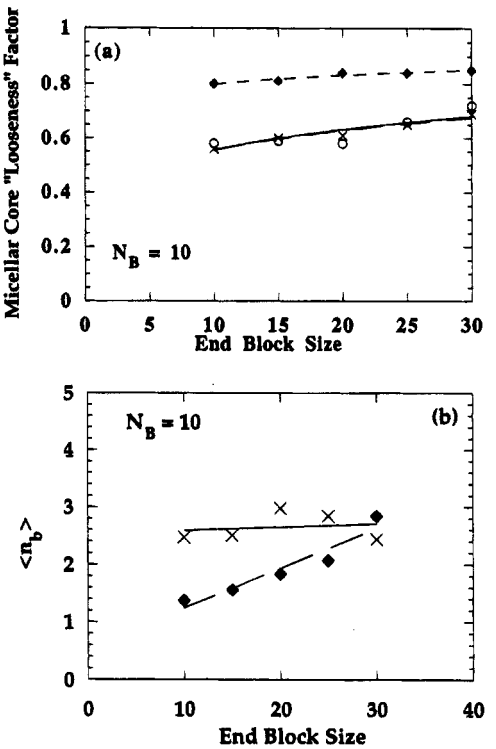

Figure 9. Effects of N_A on (a) the micellar core "looseness" factor and (b) $\langle n_b \rangle$ for $N_B = 10$ and $\{\phi, 2N_A\beta\epsilon\} = \{0.038, 30\}$ (○), $\{0.094, 30\}$ (×), and $\{0.094, 9\}$ (◆).

lifetime decreases slightly, then levels off, as ϕ increases. The bridging lifetime remains small and insensitive to ϕ at $\beta\epsilon = 0.1$, due to the high rates of transitions from bridges to loops and dangling ends.

c. Effects of the End Block Size. Panels a and b of Figure 9 depict the effects of N_A on the looseness factor and $\langle n_b \rangle$, respectively. In all of these runs, in varying N_A, $\beta\epsilon$ was also changed to keep $2N_A\beta\epsilon$ constant. The lines shown in those figures are from the best power-law fits to the data. As N_A increases, our results

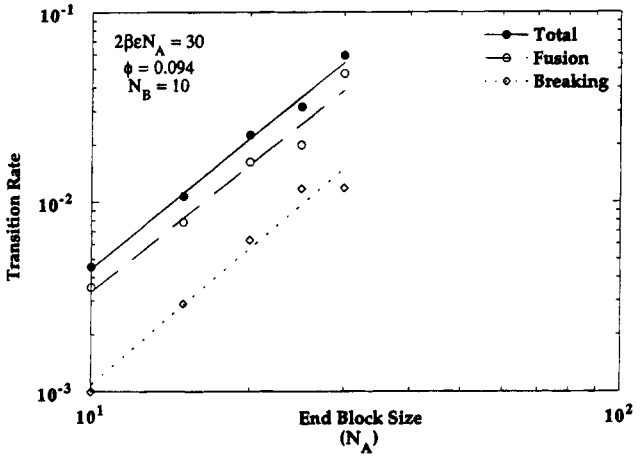

Figure 10. Variations in transition rate with N_A for $\phi = 0.094$, $N_B = 10$, and $2N_A\beta\epsilon = 30$. The lines are the best power-law fits.

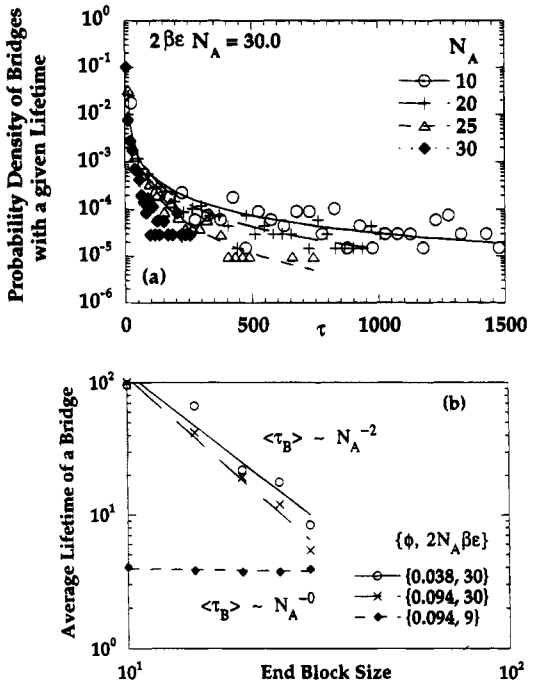

Figure 11. (a) Normalized probability density of a bridge with a given lifetime τ, for $2N_A\beta\epsilon = 30$ and various values of N_A. (b) $\langle\tau_B\rangle$ as a function of N_A.

show that p increases. Panel a of Figure 9 indicates that the looseness factor is very weakly dependent on N_A, at constant $2N_A\beta\epsilon$. The micellar cores become slightly less compact, or more loose, as N_A increases. Furthermore, as N_A increases, the bridging fraction also increases. Accordingly, panel b of Figure 9 shows that $\langle n_b\rangle$ increases with increasing end block size.

Figure 10 shows the effects of end block size on the transition rates, for $2N_A\beta\epsilon = 30$ and $\phi = 0.094$. The transition rates, at $2N_A\beta\epsilon = 9$, are larger in magnitude but exhibit similar qualitative trends. As N_A increases, the micelles become less compact and Figure 10 shows an increase in the breaking rate. The fusion rate also increases with increasing end block size, due to the increase in the core radius and the micelle aggregation number, p. Consequently, the total transition rate increases, as N_A increases. The lifetime distributions, for various N_A with $2N_A\beta\epsilon = 30$ and $\phi = 0.094$, and the average bridging lifetime are shown in panels a and b, respectively, of Figure 11. (The lifetime distribution is relatively insensitive to N_A, at $2N_A\beta\epsilon = 9$). Panel a illustrates that the distribution decays at a faster rate,

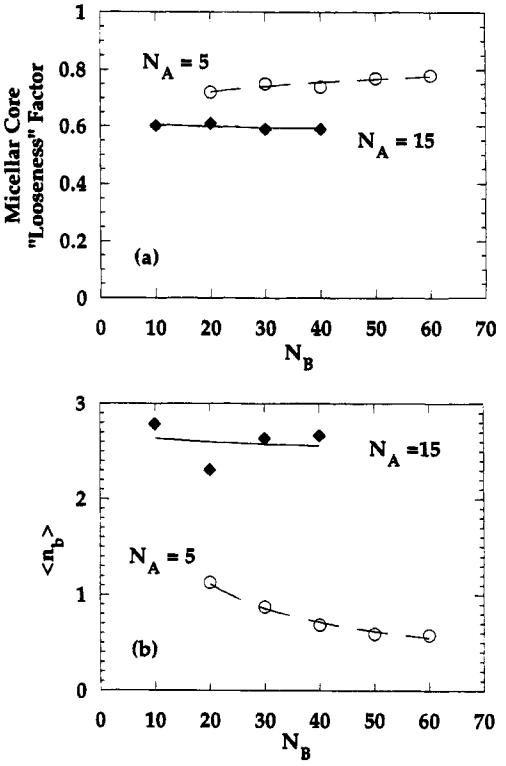

Figure 12. Effects of N_B on (a) the micellar core "looseness" factor and (b) $\langle n_b\rangle$ for $\phi = 0.094$, $\beta\epsilon = 1.0$, and $N_A = 5$ (○) and 15 (◆).

as N_A increases. Accordingly, as N_A increases, we see a strong decrease in the average bridging lifetime, at $2N_A\beta\epsilon = 30$, but essentially no change in $\langle\tau_B\rangle$, at $2N_A\beta\epsilon = 9$. These results are counterintuitive, as one would expect that the average bridging lifetime increases with increasing N_A.

d. Effects of the Middle Block Size. The middle block size effects on the looseness factor and $\langle n_b\rangle$ are illustrated for two different end block sizes ($N_A = 5$ and 15) in panels a and b of Figure 12, respectively, with $\phi = 0.094$ and $\beta\epsilon = 1.0$. As N_B increases, p decreases for both end block sizes, while n decreases significantly when $N_A = 5$ but only slightly at larger N_A. The compactness of the micellar cores does not change much with N_B, at strong incompatibility, but decreases slightly as N_B increases, at weak incompatibility (panel a of Figure 12). This is possibly due to the competing effects of decreasing loop fraction (looseness factor decreases due to decreasing excluded volume) and decreasing micellar association number (looseness factor increases due to greater exposure to solvent). In panel b of Figure 12, we see that $\langle n_b\rangle$ remains relatively constant for the larger end block size while $\langle n_b\rangle$ decreases for the smaller end block size, as N_B increases.

In Figure 13, the transition rates are depicted as functions of the middle block size, N_B, for $N_A = 15$. We see a slight increase in the breaking rate and a decrease in the fusion rate as N_B increases (due to a corresponding decrease in $\langle n_b\rangle$ and p and an increase in the intermicellar distance). The overall effect is a decrease in the total rate, with increasing N_B. The distribution of bridging lifetimes is insensitive to N_B at $N_A = 5$ but it occurs on slower time scales as N_B increases, for $N_A = 15$ (panel a of Figure 14). Correspondingly, as N_B increases, $\langle\tau_B\rangle$ increases for $N_A = 15$, but remains nearly constant at $N_A = 5$ (panel b of Figure 14).

2. Stress Relaxation. In this section, we discuss the consequences of the bridging lifetime distributions

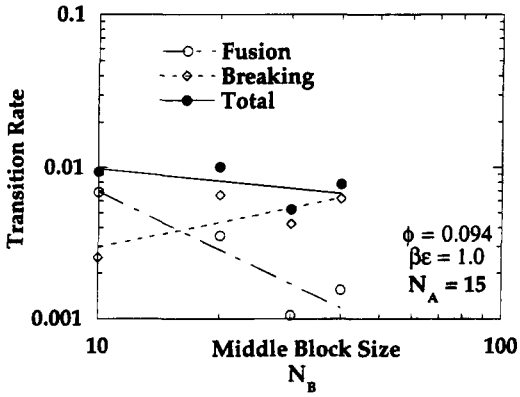

Figure 13. Variations in transition rate with N_B for $\phi = 0.094$, $N_A = 15$, and $\beta\epsilon = 1.0$. The lines are the best power-law fits.

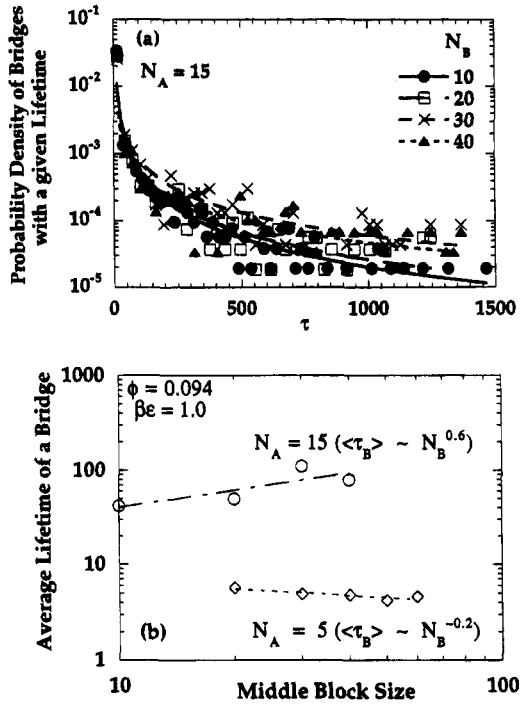

Figure 14. (a) Normalized probability density of a bridge with a given lifetime τ, for $\beta\epsilon = 1.0$ and various values of N_B. (b) $\langle\tau_B\rangle$ as a function of N_B.

on the shear stress relaxation after a unit shear strain. We assume small strain deformation so that the response is in the linear regime and small strain rate so as not to affect the conversion rates of bridges to other states. We further assume that the elastic portion of the shear stress dominates the viscous contribution by dangling and free chains (or the relaxation times of dangling and free chains are much smaller than the time scales of interest in this investigation). In other words, the stress in the system is totally due to the bridges. Of course, entangled dangling ends and entangled loops, which act essentially like bridges, could also contribute elastically. In the concentration range under investigation, which is of the order of the overlap concentration, entanglements of dangling ends are also unlikely. By visual inspection, we have seen no loop entanglements in the system under the conditions studied. The stress in the system is transferred from one cross-link site to another through the bridges, or the elastically effective chains.

At time $t = 0$ upon application of a unit shear strain the stress in the system is proportional to the number of active (bridging) chains present at the time.[38] The shear stress remaining at time $t > 0$ is just the fraction

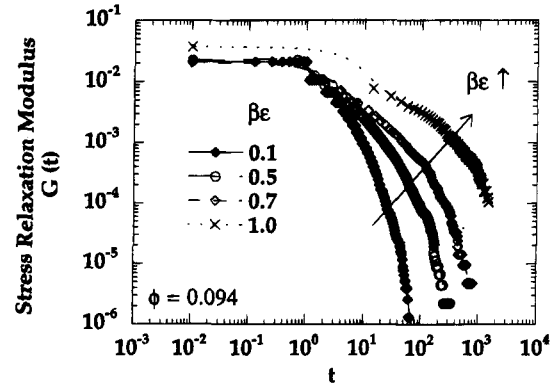

Figure 15. log–log plot of the stress relaxation modulus after a unit strain has been applied at $t = 0$, for various values of $\beta\epsilon$ with $N_A = 15$ and $N_B = 10$.

of the chains that were active at time $t = 0$, which still remain active. Although new bridges are formed as old ones are destroyed to maintain the equilibrium population of bridges, these new bridges do not contribute to the stress since they are formed after the application of strain and hence are formed in their equilibrium configurations.[11] The normalized shear stress at time t, $\sigma(t)/\sigma_0$, can be written as

$$\frac{\sigma(t)}{\sigma_0} = \sum_{\tau_i > t}^{\tau_{max}} P(\tau_i)\Delta\tau \tag{2}$$

where $\sigma(t)$ is the shear stress remaining in the system after time t has elapsed and σ_0 is the stress in the system at time $t = 0$, which is porportional to the number of bridges in the system at time $t = 0$, the equilibrium bridging density, f_b.

$$\sigma_0 = (f_b \Xi \gamma) kT \tag{3}$$

Here Ξ is the area of the surface under shear per chain (or $\Xi = M/L^2$) and f_b is the equilibrium bridging fraction. For each set of parameters, the time τ_{max} was divided into n_0 equal time intervals such that, on an average, five bridging events were observed for each interval. The fractional stress remaining at the end of a given time interval was just the fraction of bridging events that were of larger lifetimes, according to eq 2. Analytically, one can write the stress relaxation modulus, $G(t)$,

$$\frac{G(t)}{kT} = f_b \Xi \sum_{\tau_i > t}^{\tau_{max}} P(\tau_i)\Delta\tau \tag{4}$$

The relaxation modulus is a function of $\beta\epsilon$, ϕ, N_A, and N_B through its dependences on the lifetime distribution and the equilibrium bridging fraction.

In Figure 15, the effects of energy on the stress relaxation modulus are depicted for $\phi = 0.094$. This figure shows that the width of the rubbery plateau region broadens while the height slightly increases as $\beta\epsilon$ increases. These observations indicate that the contributions of the slower relaxation modes become more significant as $\beta\epsilon$ increases. Furthermore, the transition to the flow region occurs more slowly with increasing $\beta\epsilon$, as indicated by the increase in the slope in the terminal zone as $\beta\epsilon$ increases. Similar trends were observed experimentally by Stadler et al.[5-8] (for hydrogen-bonded transient networks) and Agarwal et al.[9,10] (for ionomers).

The normalized time-dependent shear stresses are shown in panel a of Figure 16 in a semilog plot for $\beta\epsilon =$

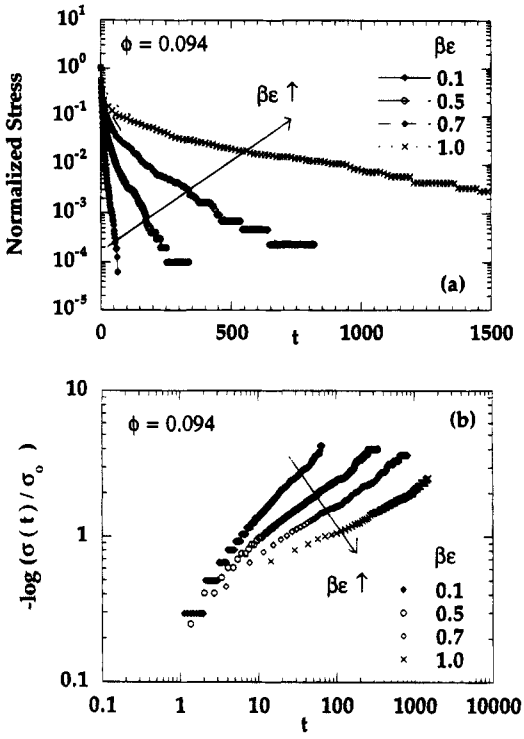

Figure 16. Normalized stress of Figure 15 shown on (a) a semilog plot of $\sigma(t)/\sigma_0$ versus t and (b) a log–log plot of $-\log(\sigma(t)/\sigma_0)$ versus t.

0.1, 0.5, 0.7, and 1.0 and $\phi = 0.094$. The fractional stress remaining at the end of a given time interval is the fraction of the total bridging events that have lifetimes greater than that time interval. Panel a of this figure clearly shows that the decay (i) is nonexponential and (ii) occurs on slower time scales as $\beta\epsilon$ increases. Again, the nonexponential decay may be a consequence of the long end blocks. The junctions (or micelles) are expected to be more complex for chains with long end blocks. For simple telechelic copolymers, specifically associative thickeners, the viscoelastic response is similar to that of a Maxwell element, i.e., exponential decay.[2]

In many random systems, such as glasses, spin-glasses, polymers, viscous fluids, and critical binary mixtures, the time evolution of the relaxation following a perturbation is highly nonexponential.[39,40] The relaxation processes in all of these systems are characterized by the broad distributions of the relaxation times. It has been suggested that the nonexponentiality arises due to the polydispersity in the relaxation time distribution. In fact, in such cases, the relaxation phenomena appears to fit a stretched exponential behavior,

$$R(t) = e^{-(t/\tau)^m} \qquad 0 < m < 1 \qquad (5)$$

where $R(t)$ is a relaxation function, τ is the mean relaxation time, and m is the stretched exponent which contains information on the shape of the distribution. (When m is 1, eq 5 is reduced to an exponential function.) The stretched exponent m may be determined by plotting $-\log(R(t))$ versus t on a log–log scale. If the function follows a stretched exponential type, this plot would be linear and m is the slope of the line. Since our system is polydisperse, we attempt fitting the stress function to a stretched exponential function. The stress decay *appears* to fit the stretched-exponential decay, at all conditions. This is illustrated in panel b of Figure 16, in which $-\log(\sigma(t)/\sigma_0)$ is plotted against t on a log–log plot and linearity was observed. In fact, there appear to be two linear regions, a faster decay at short

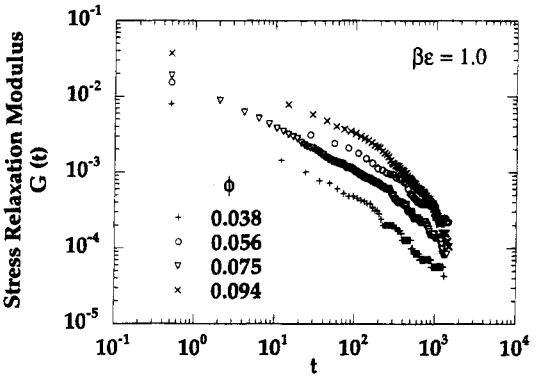

Figure 17. log–log plot of the stress relaxation modulus after a unit strain has been applied at $t = 0$, for various values of ϕ with $N_A = 15$ and $N_B = 10$.

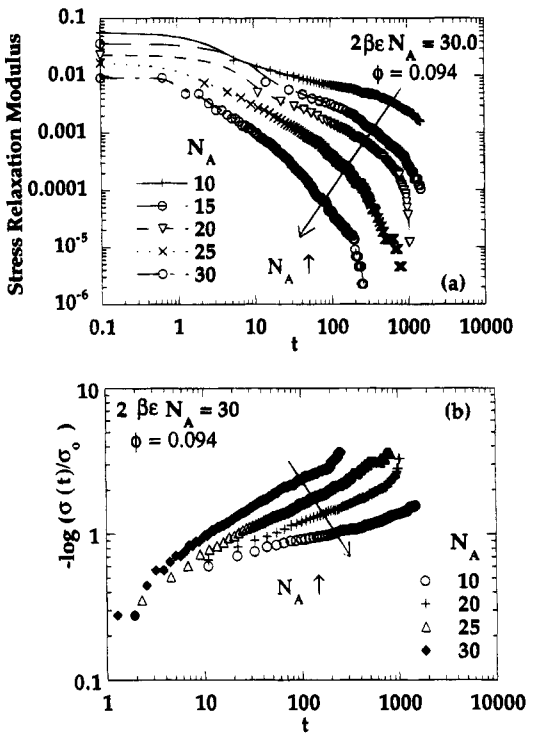

Figure 18. (a) Semilog plot of stress relaxation modulus versus t and (b) log–log plot of $-\log(\sigma(t)/\sigma_0)$ versus t, for various values of N_A.

times followed by a slower decay at longer times. The slopes in both regions decrease, as $\beta\epsilon$ increases. However, we believe that the decay may be a complex sum of several exponentials, each with its own characteristic relaxation time. Similar responses are observed in systems of triblock copolymers with adsorbing end blocks. When there is a large number of A segments associated per contact site, there are a number of steps through which these segments can disassociate. Each involves a different number of segments and thus a different relaxation spectrum is generated.

The shape of the stress relaxation function does not vary significantly with either concentration or the middle block size, but significantly with the end block size. Figure 17 illustrates the effects of concentration on the stress relaxation modulus. While the shape of the relaxation curve is insensitive to concentration, the height of the rubbery plateau increases as concentration increases (due to a corresponding increase in the number of bridges). Panels a and b of Figure 18 show that the relaxation characteristics change significantly as N_A is varied. As N_A increases, both the width and the height of the plateau region decrease. The relax-

ation occurs faster as N_A increases. Panel b of Figure 18, which is a log−log plot of $-\log(\sigma(t)/\sigma_0)$ versus t, shows that the slope increases, as N_A increases, indicating faster relaxation for triblock chains of longer end block sizes. As expected, the middle block size has very little influence on the stress relaxation of end-associated triblock copolymers.

IV. Conclusions

In this work, the relaxation dynamics of the end-associated triblock copolymers is followed, in a regime where there are no entanglements. The stress relaxation moduli, as deduced from the distributions of bridge lifetimes, are examined with specific focus on how they are affected by the system variables, particularly by the solvent quality and the end block size.

In general, the stress in such systems decays, upon an application of a unit shear strain, as bridges, which supported the stress, convert to dangling ends (via the end-breaking mechanism) and loops (via the fusion mechanism). The corresponding rates of these relaxation mechanisms depend on the surrounding environment, which in turn varies with the system variables. These rates depend strongly on the interaction energy between the end block segments and the solvent molecules ($\beta\epsilon$) and the end block size (N_A) but weakly on the middle block size (N_B) and concentration (ϕ). As $\beta\epsilon$ increases, the micelles become more compact and the breaking rate decreases significantly. On the other hand, the fusion rate passes through a maximum at an intermediate value of $\beta\epsilon$. The fusion rate and the breaking rate increase with longer end block size. The breaking rate is a function of neither the middle block size nor concentration. On the other hand, the fusion rate increases as concentration increases and decreases as the middle block size increases.

The bridge lifetime distribution does not fit a simple exponential function, leading to a stress decay that is also nonexponential. The nonexponentiality in the stress response is most likely a consequence of the polydispersity in the micelles as well as the existence of more than one relaxation pathway. As $\beta\epsilon$ increases, the lifetime distribution becomes increasingly nonexponential and its tail extends to longer lifetimes. The contributions from the slower modes become more significant as $\beta\epsilon$ increases, leading to larger average bridging lifetimes, $\langle\tau_B\rangle$. On the other hand, as the end block size gets longer, the bridges, on the average, have shorter lifetimes. The stress relaxation appears to fit a stretched-exponential function. As $\beta\epsilon$ increases, the rubbery plateau region broadens and its height increases. The transition to flow occurs more slowly (as indicated by the larger slopes in the terminal zone) with increasing $\beta\epsilon$. As the end block size increases, both the width and height of the plateau region decrease while the transition to flow occurs at a faster rate. The stress response is relatively insensitive to variations in either concentration or middle block size.

Acknowledgment. We thank S. Misra for the critical reading of this manuscript. This work was supported by National Science Foundation Grant DMR-92-20369.

References and Notes

(1) Persson, K.; Abrahmsen, S.; Stilbs, P.; Hansen, F. K.; Walderhaug, H. *Colloid Polym. Sci.* **1992**, *270*, 465.
(2) Annable, T.; Buscall, R.; Ettelaie, R.; Whittlestone, D. *J. Rheol.* **1993**, *37*, 695.
(3) Walderhaug, H.; Hansen, F. K.; Abrahmsen, S.; Persson, K.; Stilbs, P. *J. Phys. Chem.* **1993**, *97*, 8336.
(4) Rao, B.; Yoshimitsu, U.; Dyke, L.; Macdonald, P. M. *Macromolecules* **1995**, *28*, 531.
(5) Stadler, R.; de Lucca Freitas, L. L. *Colloid Polym. Sci.* **1986**, *264*, 773.
(6) de Lucca Freitas, L. L.; Stadler, R. *Macromolecules* **1987**, *20*, 2478.
(7) Stadler, R. *Prog. Colloid Polym. Sci.* **1987**, *75*, 140.
(8) Stadler, R.; de Lucca Freitas, L. L. *Macromolecules* **1989**, *22*, 714.
(9) Agarwal, P. K.; Makowski, H. S.; Lundberg, R. D. *Macromolecules* **1980**, *13*, 1679.
(10) Agarwal, P. K.; Garner, R. T.; Graessley, W. W. *J. Polym. Sci., Part B: Polym. Phys. Ed.* **1987**, *25*, 2095.
(11) Green, M. S.; Tobolsky, A. V. *J. Chem. Phys.* **1945**, *14*, 80.
(12) Lodge, A. S. *Trans. Faraday Soc.* **1956**, *52*, 120.
(13) Yamamoto, M. *J. Phys. Soc. Jpn.* **1956**, *11*, 413.
(14) Tanaka, F.; Edwards, S. F. *J. Non-Newtonian Fluid Mech.* **1992**, *43*, 247.
(15) Tanaka, F.; Edwards, S. F. *J. Non-Newtonian Fluid Mech.* **1992**, *43*, 273.
(16) Tanaka, F.; Edwards, S. F. *J. Non-Newtonian Fluid Mech.* **1992**, *43*, 289.
(17) Tanaka, F.; Edwards, S. F. *Macromolecules* **1992**, *25*, 1516.
(18) Wang, S.-Q. *Macromolecules* **1992**, *25*, 7003.
(19) Baxandall, L. G. *Macromolecules* **1989**, *22*, 1982.
(20) Gonzalez, A. E. *Polymer* **1983**, *24*, 77.
(21) Gonzalez, A. E. *Polymer* **1984**, *25*, 1469.
(22) Leibler, L.; Rubinstein, M.; Colby, R. H. *Macromolecules* **1991**, *24*, 4701.
(23) Graessley, W. W. *Adv. Polym. Sci.* **1982**, *47*, 67.
(24) Nguyen-Misra, M.; Mattice, W. L. *Macromolecules* **1995**, *28*, 1444.
(25) Binder, K. In *Computational Modeling of Polymers*; Bicerano, J., Ed.; Marcel Dekker: New York, 1992.
(26) Binder, K. *Adv. Polym. Sci.* **1994**, *112*, 181.
(27) Misra, S.; Nguyen-Misra, M.; Mattice, W. L. *Macromolecules* **1994**, *27*, 5037.
(28) Anniasson, E. A. G.; Wall, S. N. *J. Phys. Chem.* **1974**, *78*, 1024.
(29) Anniasson, E. A. G.; Wall, S. N.; Almgren, M.; Hoffmann, H.; Kielmann, I.; Ulbricht, W.; Zana, R.; Lang, J.; Tondre, C. *J. Phys. Chem.* **1976**, *80*, 905.
(30) Halperin, A. *Europhys. Lett.* **1989**, *8*, 351.
(31) Halperin, A.; Alexander, S. *Macromolecules* **1989**, *22*, 2403.
(32) Witten, T. A. *J. Phys. Fr.* **1988**, *49*, 1055.
(33) Johner, A.; Joanny, J.-F. *Europhys. Lett.* **1991**, *15*, 265.
(34) Dai, L.; Toprakcioglu, C. *Europhys. Lett.* **1991**, *16*, 331.
(35) Milner, S. T.; Witten, T. A. *Macromolecules* **1992**, *25*, 5495.
(36) Dai, L.; Toprakcioglu, C. *Macromolecules* **1992**, *25*, 6000.
(37) Wijmans, C. M.; Leermakers, F. A. M.; Fleer, G. J. *J. Colloid Interface Sci.* **1994**, *167*, 124.
(38) Treloar, L. R. G. *The Physics of Rubber Elasticity*; Clarendon Press: Oxford, U.K., 1975.
(39) Piazza, R.; Bellini, T.; Degiorgio, V. *Phys. Rev. B* **1988**, *38*, 7223.
(40) Bellini, T.; Mantegazza, F.; Piazza, R.; Degiorgio, V. *Europhys. Lett.* **1989**, *10*, 499.

MA950667J